COMMUNICATION

Switching effective oxygen reduction and evolution performance by controlled graphitization of a cobalt–nitrogen–carbon framework system†

Srinivas Gadipelli,* Tingting Zhao, Stephen A. Shevlin and Zhengxiao Guo*

We report a purposely designed route for the synthesis of a promising carbon-based electrocatalyst for both ORR (oxygen reduction reaction) and OER (oxygen evolution reaction) from zeolitic imidazolate frameworks (ZIFs). Firstly, precursor ZIFs are rationally designed with a blend of volatile zinc to induce porosity and stable cobalt to induce graphitic domains. Secondly, the self-modulated cobalt–nitrogen–carbon system (SCNCS) is shown to be an effective ORR catalyst after graphitization at mild temperatures. Finally, the best OER catalyst is developed by enhancing graphitization of the SCNCS. For the first time, solely by switching the graphitization conditions of SCNCS, excellent ORR or OER performance is realized. This approach not only opens up a simple protocol for simultaneous optimization of nitrogen doping and graphitization at controlled cobalt concentrations, but also provide a facile method of developing such active catalysts without the use of extensive synthesis procedures.

Broader context

Electrochemical energy storage and conversion technologies, such as fuel-cells, rechargeable metal–air batteries and water electrolysers are highly desirable for electric vehicles, distributed power supply, integration of renewables and energy balancing in electricity grids. However, high cost has been a major obstacle hindering their wide spread applications, nearly 40% of which is due to the use of expensive catalysts. Hence, a critical challenge is to identify cost-effective electrocatalysts for the oxygen reduction and evolution reactions (ORR and OER), to replace platinum and iridium oxide, respectively. Here, we report an approach of obtaining highly effective ORR and OER electrocatalysts based on nanoporous functionalised carbon of a cobalt–nitrogen–carbon framework system. For this highly porous, bimetallic precursor, zeolitic-imidazolate frameworks (Co_xZn_{100-x}) are rationally designed, and subjected to different carbonization conditions. The optimized system is identified through extensive screening of samples obtained at different synthesis conditions, such as cobalt- and nitrogen-concentrations, degree of graphitization, porosity and oxidation state of cobalt. Finally, we show that the tuneable catalytic activity for ORR and OER can be achieved by relatively simple control over cobalt concentration and cobalt-induced graphitization. This approach points to a new direction in the design and development of cost-effective electrocatalysts.

Energy storage and conversion technologies are critical for clean transport and renewable integration in smart grids.[1,2] Nanoporous solids play a vital role in such technologies, including catalysis, charge-carrier storage and molecular sorption and separation.[3–8] In particular, nanoporous carbons (NPCs) are highly desirable for such purposes, due to their high accessible specific surface area and pore volume, high chemical and mechanical stabilities, and good electrical conductivity.[3,6–10] Functionalised NPCs are considered an emerging group of non-noble metal oxygen reduction and evolution electrocatalysts in fuel-cells and metal–air batteries.[9–24] For example, nitrogen or sulphur doping and/or incorporation of transition metals in the carbon lattice induce significant surface charge and graphitization to enhance charge transfer capacity. Increasing accessible porosity (specific surface area (SSA), pore-size distribution (PSD) and pore volume (V_p)) of the NPCs facilitates fast mass or charge-carrier transfer. These properties can be enhanced with the selection of appropriate
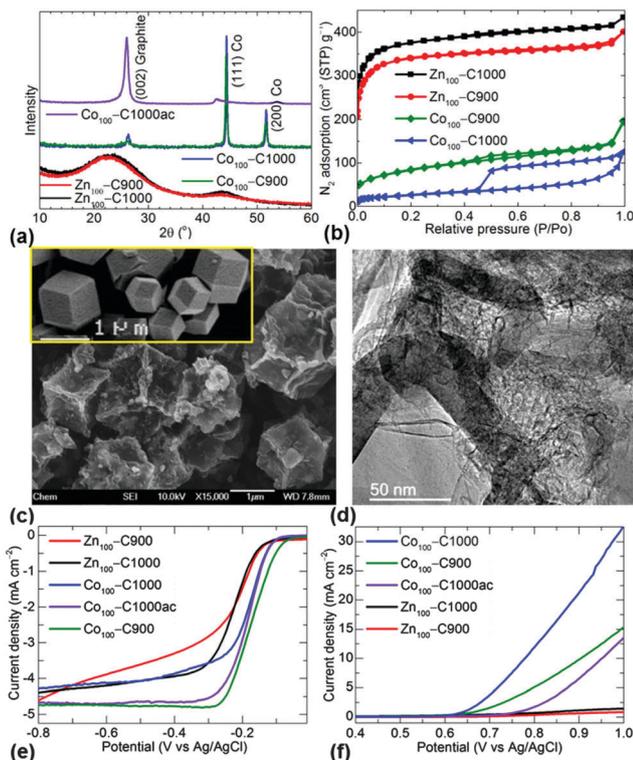
carbon precursors or chemical synthesis routes. Therefore advances in synthesis lead to new classes of functional NPCs. Carbon nanotube/graphene/graphene-oxide based metal–nitrogen–carbon structures are recent examples of such NPCs that show superior catalytic activities for ORR or OER, compared with expensive Pt or Ir and Ru oxides.[9–11,13–18] However, developing such graphene/nanotube based NPCs usually involves extensive chemical processes, thus hindering large scale commercial implementation.

In contrast, the intrinsically open pore polymers with metal cores as sacrificial templates have proved extremely advantageous for the development of multifunctional NPCs.[4,5,7,22–29] The best example of such templates are metal–organic frameworks (MOFs), which consist of small ligand molecules as linkers with metal centres to produce regularly ordered open frameworks of a high specific surface area.[4,5] The carbonization of MOFs yields a new class of highly porous NPCs with simultaneous incorporation of intrinsic ligand heteroatoms and metal centres within the

Department of Chemistry, University College London, 20 Gordon Street, London, WC1H 0AJ, UK. E-mail: gsrinivasphys@gmail.com, z.x.guo@ucl.ac.uk

This journal is © The Royal Society of Chemistry 2016

Energy Environ. Sci., 2016, 9, 1661–1667 | 1661

Fig. 1 The structure property characteristics of NPCs derived from ZIF-8 and -67 alone at 900 °C for 6 h and 1000 °C for 10 h: (a) PXRD patterns. (b) 77 K N_2 adsorption–desorption isotherms. (c) SEM images of Co_{100}–C1000-10h and Zn_{100}–C1000-10h (inset). (d) TEM image of Co_{100}–C1000ac-10h. (e and f) Electrocatalytic activity of NPCs in O_2 saturated 0.1 M KOH at a scan rate of 10 mV s^{-1}; LSV curves for ORR at 1600 rpm (e) and LSV curves for OER at 1600 rpm (f). Note that in order to compare with zinc-metal free Zn_{100}–C1000, the Co_{100}–C1000ac is presented after acid clean (denoted with "ac") to remove cobalt-metal.

carbon matrix.[7,22–29] The advantage of this approach is that functional and conducting NPCs can be easily developed from rationally designed MOFs, e.g. MOF-5 and ZIF-8.[30,31] Imidazolate ($H_3C_3N_2$) ligand based ZIFs, a sub family of MOFs with zeolitic structure, deserve a special mention. With the choice of enriched volatile (e.g., Zn) or stable (e.g., Fe, Co, Ni) metal centres, these ZIFs can generate metal free or metal-incorporated nitrogen-doped carbons with a significant degree of graphitization (see references Sb1–9, Sc1–22, Sd1–5 and Se1–12 in the ESI†).[22–28]

More precisely, as shown in Fig. 1 and Fig. S1–S5 (ESI†), the carbonization of ZIF-8 (Zn_{100}–C) and Co–ZIF-8 (Co_{100}–C) exhibits different structure and porosity characteristics. Zn_{100}–C NPCs are mainly amorphous in nature and exhibit a higher level of microporosity and nitrogen doping (Tables S1 and S2, ESI†). At similar synthesis conditions Co_{100}–C results in more graphitized mesoporous NPCs with embedded crystalline cobalt. This graphitization is further confirmed by scanning and transmission electron microscopy (SEM and TEM) micrographs. Clearly, the graphitized Co_{100}–C1000 after acid clean to remove cobalt metal shows enhanced electrocatalytic activity for both the ORR and OER compared with the amorphous Zn_{100}–C1000 counterpart without zinc (Fig. 1e and f). For example, the ORR activity is observed by a well-defined and sharp cathodic current peak at an

applied potential of around −0.15 V vs. Ag/AgCl. This is not observed in the N_2 purged electrolyte (Fig. S6, ESI†). The enhanced ORR performance of Co_{100}–C NPCs is also characterised by reduced onset and half-wave potentials, electron transfer and a steep reduction slope, i.e., a reduced Tafel slope (Fig. S6–S8, ESI†) with enhanced current density against sweeping potential. Furthermore, a considerable enhancement in OER activity is seen in the cobalt incorporated NPCs (Fig. S9, ESI†).

Interestingly, the thermogravimetric analysis of C_{100}–C1000 accounts for 44% of cobalt by mass (Fig. S10, ESI†). This is very high and expected to limit the catalytic activity due to poor dispersion of active sites. Also note that the graphitized NPCs with or without cobalt at minimal nitrogen doping exhibits improved ORR and OER activities than the highest nitrogen doped amorphous NPCs. Thus we anticipate that fine control over graphitization, and nitrogen and cobalt concentrations would result in further improved catalytic activity of these NPCs.[12–27]

In principle, a precursor ZIF, designed rationally with a blend of volatile zinc to induce porosity and stable cobalt to induce graphitic domains, can generate optimized NPCs. This strategy also enhances the fine distribution of the active sites. For example, cobalt centres, facilitate fast electron-transfer kinetics for OER/ORR. In general, a higher effective surface area leads to higher electrocatalytic activity. However, research along this line has not been well explored.[22,27] Also in most of the cases the MOF- or ZIF-derived NPCs were considered for ORR but rarely for OER [see references in the ESI†]. This is because most of those MOFs or ZIFs were subjected to a mild carbonization temperature and less annealing time. Thus, as demonstrated in Fig. 1, these structures exhibit very poor or no activity for OER. Furthermore, the range of graphitization conditions and metal concentrations for NPCs (other than the inherent metal of the MOF or ZIF) and their viability for complete electrocatalysis are yet to be explored.

Therefore, here we have performed a detailed investigation to explore the potential of these ZIF-based NPCs with a targeted synthesis from rationally designed bimetal (Co_xZn_{100-x})–ZIF-8 (Fig. 2 and Fig. S11–S13, ESI†). The bimetal ZIFs are converted to functionalized NPCs with a direct carbonization between (700–1100) °C with annealing for (2–10) h, i.e., mild to high graphitization under pure or control oxidative N_2 atmosphere. The optimized NPCs are identified through extensive screening of samples obtained at different synthesis conditions, such as controlled cobalt- and nitrogen-concentrations, degree of graphitization, porosity and oxidation state of cobalt (Co(0)/C, Co(II)O@Co(0)/C and Co_3(II, III)O_4/C). Thus obtained NPCs are investigated for both ORR and OER activities directly without further chemical/acid treatment. Throughout the text NPCs are named against the MOF type, and carbonization temperature and time, for example, Co_xZn_{100-x}–ZIF-8 carbonized at 1000 °C for 10 h is named as Co_xZn_{100-x}–C1000-10h. The NPCs are thoroughly characterized with complementary techniques, such as powder X-ray diffraction (PXRD), Raman spectroscopy, X-ray photoemission spectroscopy (XPS), electron microscopy (SEM and TEM), thermogravimetry and porosity (N_2, CO_2 and H_2 uptake), see Fig. 3 and Fig. S14–S28, and Tables S3 and S4 (ESI†). An overview of structure–property
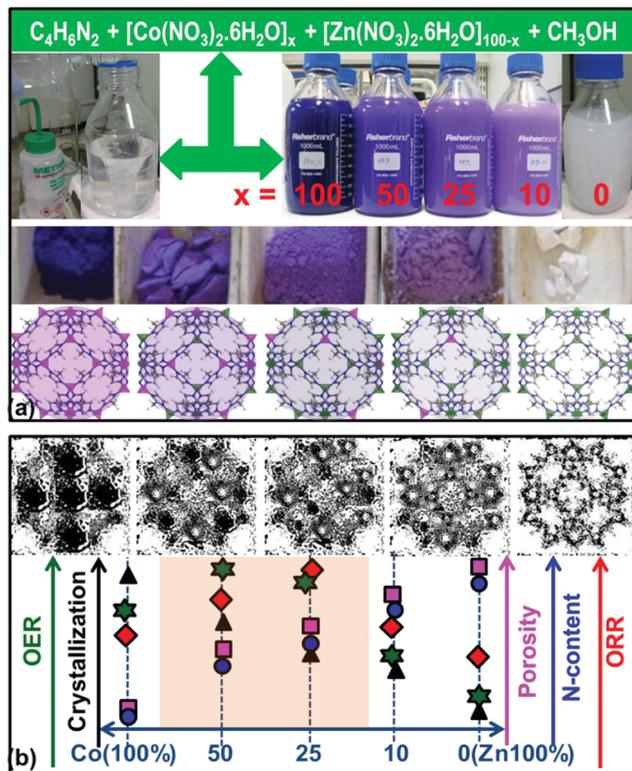
Fig. 2 Synthesis, structural and electrochemical characteristics of ZIFs and NPCs: (a) sample preparation of Co_xZn_{100-x}–ZIF-8 with a different precursor and metal salt concentrations, x = 100, 50, 25, 10 & 0, respectively, represents from left to right. The precursor solution mixtures in bottles (top row) and ZIF powders (middle row), and local pore structures (bottom row), respectively are represented with digital photographs and wire-frames of ligand and metal-centres. Colour codes: grey-carbon, blue-nitrogen, white-hydrogen, pink-cobalt, and green-zinc. (b) Characteristic, structure–property relationships of carbonized products of Co_xZn_{100-x}–ZIF-8. Note that evaporation of zinc metal (at ∼910 °C) results remains open framework, high porosity, and amorphous carbon structure. Continuous introduction of cobalt metal results in cobalt embedded (black spots), graphitized structure of reduced porosity and nitrogen (N)-content. The best ORR and OER properties are observed at intermediate cobalt/zinc concentrations.

relationships is shown schematically in Fig. 2b. Clearly, the rationally designed Co_xZn_{100-x}–ZIF-8 (x = 25 and 50) derived NPCs show outstanding activity for both ORR and OER (Fig. 2b and Fig. S29, ESI†). More specifically, graphitization acts as a switch for high activity; ORR at ≤900 °C and OER at ≥1000 °C. We note that several factors play a decisive role, such as cobalt and nitrogen concentration, and graphitization temperature. We also note that the NPCs reported here are obtained by direct carbonization of ZIFs alone. In contrast, the literature often reports the addition of extra functional precursors, graphene or template support directed growth, and pre- and/or post-synthesis treatment [see references Sb1–9, Sc1–22, Sd1–5 and Se1–12 in the ESI†]. Furthermore, as noted above the literature ZIF-carbons with high nitrogen content show a good ORR performance but have rarely being investigated for OER or clearly show poor or no activity for OER, see Fig. 1, 2 and Fig. S30 (ESI†).

The PXRD patterns of the NPCs show a clear transition from amorphous carbon to graphitized carbon with increasing substitutional cobalt for zinc (Fig. 3a and Fig. S14, ESI†). Carbonization temperature also plays a vital role in enhancing the crystallinity of carbon. Graphitization is also observed by sharp Raman D and G bands when going from Zn_{100}–C to Co_{100}–C (Fig. S15, ESI†).[32,33] The XPS core level C 1s peak at binding energy of ≈285.1 eV is assigned to nitrogen doped sp^2 carbons,[28,34] for NPCs obtained at ≤800 °C (Fig. 3b and Fig. S16–S18 and Table S3, ESI†). A transformation to a pure graphitic sp^2 carbon phase with increasing temperature is suggested by a gradual narrowing and shift of a peak to a binding energy of 284.6 eV (see deconvolution).[28,29,34] The Co 2p spectra show mainly surface oxidation and nitrogen coordination. Note that in a control experiment, the oxidation of the samples to yield Co_3O_4/carbon shows different Co 2p and O 1s spectral peaks (Fig. S16–S19, ESI†).

N_2, H_2 and CO_2 molecular uptake isotherms of NPCs reveal a gradual reduction of microporosity with increasing substitutional cobalt (Fig. 3c and Fig. S20–S24 and Table S4, ESI†). A reasonable retention of porosity (≈500 m² g⁻¹ and 0.5 cm³ g⁻¹) is obtained at intermediate cobalt concentrations. It is worth noting that all the precursor ZIFs show a similar open pore framework structure
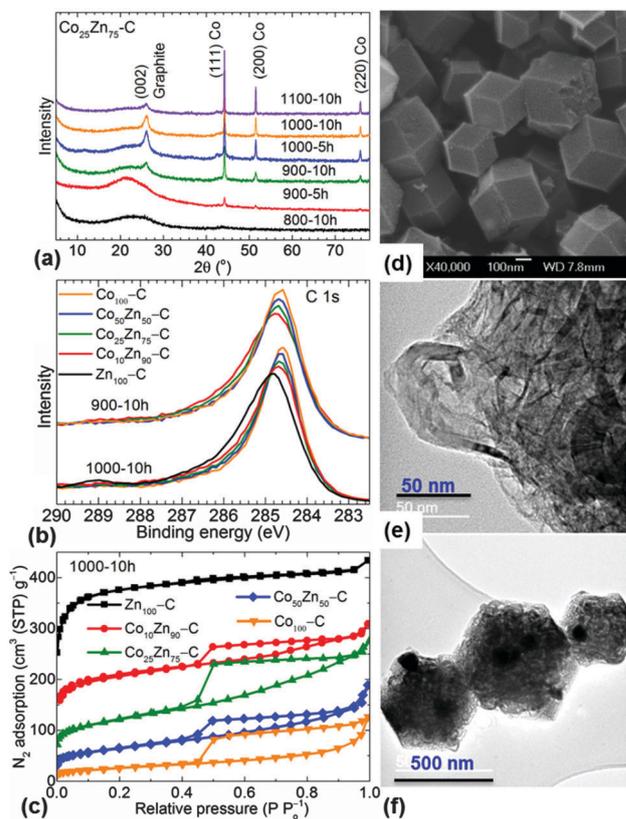

Fig. 3 Structural characteristics of Co_xZn_{100-x}–NPCs: (a) PXRD diffraction patterns of $Co_{25}Zn_{75}$–C at different temperature and period. (b) C 1s XPS core level spectra of Co_xZn_{100-x}–C900-10h and Co_xZn_{100-x}–C1000-10h, the same colour code applies for the plots. (c) 77 K N_2 adsorption–desorption isotherms of Co_xZn_{100-x}–C1000-10h. (d) SEM image of $Co_{25}Zn_{75}$–C1000-10h. (e and f) TEM images of $Co_{25}Zn_{75}$–C1000-10h at different magnifications.

(Fig. S11, ESI†). Most of the graphitized Co_xZn_{100-x}–NPCs are mesoporous in nature with a single pore diameter of ~ 5 nm. The uneven trend in the porosity with respect to the carbonization temperature between (700 and 1100) °C is directly linked to the framework decomposition at ≤ 700 °C and the competition between subsequent ligand decomposition, cobalt-induced graphitization at ≥ 700 °C, and also the vaporization of zinc at > 900 °C (Fig. S27, ESI†).[28,29] H_2 and CO_2 uptake behaviour is directly attributed to the microporosity, and the inherent active nitrogen and metal-centres.[6,28,35–37]

In the SEM and TEM images a clear transformation to highly graphitized carbon is observed with increasing cobalt substitution (Fig. 3d–f and Fig. S3–S5, S12, S13, S25 and S26, ESI†). The TEM images of $Co_{25}Zn_{75}$–C800-10h show finely distributed cobalt and zinc metal centres within the disordered carbon, whereas $Co_{25}Zn_{75}$–C1000-10h show some clustering of cobalt and nanoribbons of carbon in locally graphitized carbon structure. For the first time the extent of graphitization is further analysed with the oxidation of carbon using thermogravimetric analysis under flowing air (Fig. S28, ESI†). With increasing temperature the Co_xZn_{100-x}–C1000-10h and Co_xZn_{100-x}–C1100-10h samples show different behaviours for mass loss. This is directly attributed to the different thermal stabilities associated with the amorphous and crystalline carbon. The cobalt-induced graphitization is evidenced by two-stage mass loss at ~ 300 °C (burning off of amorphous carbon) and ~ 400 °C (burning off of graphitized carbon) in Co_xZn_{100-x}–C1000 samples. The samples with $x = 25$ and 50 consists of (60–80)% graphitized carbon. The residual mass at 700 °C estimates about (10–44)% cobalt by mass with respect to the carbon and nitrogen in Co_xZn_{100-x}–C1000.

The chemical and structural transitions going from ZIF-8 to functionalized NPCs via framework and ligand decomposition[35] are further demonstrated with a combined thermogravimetry and mass spectrometry analysis (Fig. S27, ESI†). A framework decomposition/carbonization temperature is seen at ≈ 600 °C, and evolution of various decomposed gaseous mixtures; C, C_xH_y, C_xN_y or both, $H_zC_xN_y$. Evidently, the increased cobalt substitution for zinc leads to a rapid ligand decomposition at reduced temperatures than in Zn–ZIF-8. The residual mass at the 1000 °C isothermal step is in good agreement with the selected precursor composition to synthesize ZIFs. For example, each 50% increase in cobalt substitution for zinc shows an equally enhanced residual mass of $\sim 14\%$. We also note that there is a large yield of NPCs, especially close to 50% by mass with respect to the bimetal ZIF-8. This is higher compared to the polymeric or biomass derived activated carbons.[29,36]

Next, the ORR and OER catalytic activity of the optimized NPCs is demonstrated, see Fig. 4 and Fig. S30–S40 and Tables S5 and S6 (ESI†). The carbonization temperature and thus graphitization, substitutional cobalt, nitrogen content and porosity in the samples play a key role in exhibiting high activities for both ORR and OER. For example, for the samples carbonized at ≤ 800 °C, a considerably enhanced ORR activity is seen when going from cobalt-free to cobalt-substituted carbons (Fig. S30, ESI†). This is characterized in terms of onset potential, half-wave reduction potential, Tafel slope, limiting current density and number of
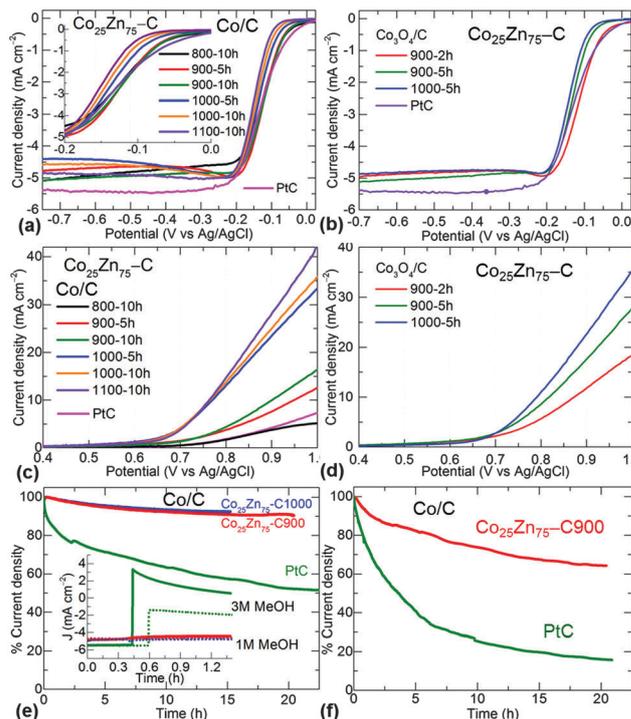

Fig. 4 Electrochemical catalytic activity of $Co_{25}Zn_{75}$–NPCs: (a–d) ORR (a and b) and OER (c and d) LSV (at 1600 rpm and scan rate of 10 mV s^{-1} in 0.1 M KOH electrolyte) curves at different carbonization conditions. Inset of (a) is expanded scale to show the difference in the onset potential. (e and f) ORR stability (current density, J vs. time) response of $Co_{25}Zn_{75}$–C900-10h and $Co_{25}Zn_{75}$–C1000-10h with a reference Pt/C in alkaline (0.1 M KOH) (e) and acidic (0.1 M $HClO_4$) (f) electrolyte. Inset of (e) is a stability response of $Co_{25}Zn_{75}$–C900-10h and Pt/C after addition of 1.0 M (dotted line) and 3.0 M (solid line) methanol into KOH electrolyte. The samples synthesized in inert atmosphere and control oxidation are represented with Co/C (a, c, e and f) and Co_3O_4/C (b and d), respectively.

electron transfer steps. The highest ORR performance is obtained for the samples carbonized at 900 °C. Similarly, continuous improvement in the OER performance is seen with respect to cobalt-induced graphitization when increasing the carbonization temperature up to 1100 °C. Clearly, the carbonization temperature strongly influences ORR and OER activities – with 900 °C as the switching point for benefiting ORR or OER. More precisely, enhanced ORR ≤ 900 °C/1000 °C $\geq$ enhanced OER. For ORR activity a volcano behaviour is seen when going from 700 °C to 1100 °C with 900 °C being the optimal synthesis temperature.[9] Similar behaviour is also observed when going from Zn_{100}–C to Co_{100}–C NPCs with $Co_{25}Zn_{75}$–C being an optimal structure at any given temperature.

A remarkable ORR performance is obtained with further tuning of carbonization conditions, such as controlling the period of carbonization and oxidation of cobalt to Co_3O_4 within the carbon matrix. As shown in Fig. 4a–d and Fig. S30–S32 (ESI†), the Co/C-5h and Co_3O_4/C-2h samples derived from $Co_{25}Zn_{75}$–ZIF-8 show better (steep slope/half-wave potentials and electron transfer number) or equivalent (onset potential and limiting current density) ORR performance to that of a reference Pt/C. The electron transfer number between 3.8 and

4.0, suggesting a 4-electron reaction pathway for Co_xZn_{100-x}–NPCs, similar to Pt/C (O_2 is reduced to OH^-) (Fig. S33, S34 and Table S5, ESI†).[11] Note that ZIF-8 or ZIF-67 alone derived NPCs are less likely to involve a 4-electron process (Fig. S8, ESI†). Increased surface oxide thickness, *i.e.*, CoO@Co/C results in a reduced ORR activity (Fig. S35, S36 and S41).[38]

The stability of the NPCs, *i.e.* retention of a high current density against continuous operation, up to 20 h is further tested in both alkaline and acidic media (Fig. 4e, f and Fig. S37, ESI†). The $Co_{25}Zn_{75}$–C900-10h sample shows 9% and 36% drop in current density compared with 48% and 84% drop for Pt/C, respectively in 0.1 M KOH and 0.1 M $HClO_4$.[23] In particular, $Co_{25}Zn_{75}$–C900-10h maintains high stability in acidic medium than Pt/C. Furthermore, the NPCs show higher methanol oxidation tolerance than Pt/C. The Tafel plot slopes (Fig. S38, ESI†) and half-wave potentials (Table S6, ESI†) reveal that a high degree of graphitization is beneficial for fast reaction kinetics. The slope and half-wave potentials are continuously reduced with increasing carbonization temperature from 900 °C to 1100 °C. In contrast, the best positive onset potentials are observed at 900 °C with desired pyridinic and graphitic nitrogen functionality. Most of the samples exhibit faster reaction rates than Pt/C (Fig. S38 and Table S6, ESI†). The smaller Tafel slopes (48–50) mV decade^{-1} and half-wave potentials (*e.g.*, 45 mV) are seen for Co_xZn_{100-x}–C1100 ($x = 10$ and 25) compared to the high nitrogen content NPCs (at 900 °C) and Pt/C (82 mV decade^{-1} and 72 mV). These experimental observations are further probed by density functional theory calculations (see ESI,† Fig. S42). These show that the addition of cobalt–nitrogen dopants render the ORR process exothermic.

A remarkable OER performance of NPCs is observed at a controlled cobalt concentration in the Co_xZn_{100-x}–NPCs (Fig. 1f, 4c–d and Fig. S9 and S30–S32, ESI†). The highest cobalt containing ZIF-67 derived carbon shows limited OER performance. Carbonisation temperature/graphitization and cobalt concentration strongly influences OER activity. The $Co_{50}Zn_{50}$–NPCs show the highest OER activity at any given carbonization condition among all the NPCs. At a benchmark current density of 10 mA cm^{-2}, the best OER performance is observed at a potential of $\approx$(0.72–0.76) V *vs.* Ag/AgCl (or 1.67–1.71 V *vs.* RHE, reversible hydrogen electrode) for the Co_xZn_{100-x}–C1000/1100 ($x = 25$ and 50). These potentials are very close to or better than the benchmark OER material, IrO_2/C with 1.71 V *vs.* RHE.[20] Note that the best ORR active NPCs derived at mild graphitization conditions show very poor or no activity for OER. However, the same NPCs can be tuned into an effective OER or bifunctional (for both OER and ORR) catalyst by being simply subjected to high graphitization conditions.

The superior OER performance of $Co_{50}Zn_{50}$–C1100-10h is further demonstrated with stability and visible oxygen evolution, see Fig. 5 and Fig. S39 and S40 (ESI†). Improved OER performance with enhanced reaction kinetics is further observed in the Tafel plots (Fig. S40, ESI†) with smaller slopes (86–92 mV decade^{-1}) than benchmark IrO_2/C (93.2 mV decade^{-1}).[20] There is a continuous decrease in the Tafel slope with increasing cobalt concentration or carbonization temperature to facilitate fast electron transfer in the
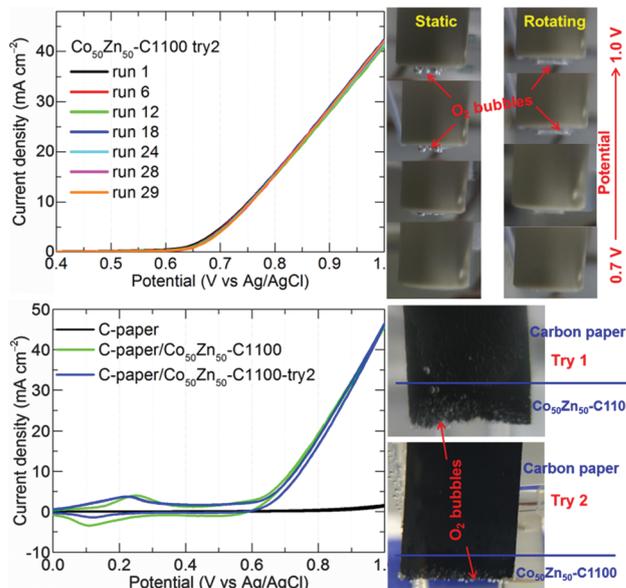

Fig. 5 OER characteristics of $Co_{50}Zn_{50}$–C1100-10h catalyst deposited on glassy carbon electrode during LSV (top) and carbon paper (C-paper) electrode during CV (bottom). The right panels are digital images recorded during the tests showing visible oxygen evolution (see gas bubbles). Note that no oxygen evolution is observed from the carbon paper without catalyst, which is also evidenced at a negligible increment in the current density. Try 2 represents the tests for freshly prepared second electrode.

graphitized structures. The onset potential of $\sim$1.57 V *vs.* RHE and potential ($\sim$1.7 V *vs.* RHE) required for generating a current density of 10 mA cm^{-2} are lower than or comparable to the best OER catalysts reported in the literature under the same experimental conditions.[9,15,18,20,21,39–44]

The literature indicates that the charge-transfer barrier and formation of O–O in the OOH adsorbate followed by deprotonation of the OOH group determines the catalytic efficiency of OER.[16] The $Co_{50}Zn_{50}$–C1100-10h sample should exhibit the lowest charge transfer resistance due to its metallic cobalt core covered with a conducting graphitized carbon shell with few defects. The transition metals with multivalent oxidation states readily participate in redox reactions.[10] The metal–nitrogen–graphite system with more graphitic nitrogen is reported to show better OER activity.[45] Furthermore, Chen *et al.* demonstrated a best OER activity from metallic Co_4N porous nanowire arrays.[40] Positively charged metal-nitrogen sites or carbons adjacent to nitrogen (due to the electron-withdrawing nature of nitrogen in graphene) facilitate the adsorption of OH^- and recombination of two adsorbed oxygens.[9,16,21,45,46] As discussed in the theoretical calculations (ESI,† Fig. S43), cobalt atoms have a large positive charge thus aiding OH^- adsorption. This single precursor based self-modulated cobalt–nitrogen–carbon system can also be considered for complete water splitting.[47]

Conclusions

In summary, we have developed a simple and facile synthesis approach to realize high performance cobalt–nitrogen–carbon

based electrocatalysts for ORR/OER. Samples derived from bimetallic Co_xZn_{100-x}–ZIF-8 at mild graphitization of 900 °C show the highest activity for ORR (and the lowest activity for OER). Balanced ORR and OER activities are obtained with further graphitization at 1000 °C while the highest activity for OER occurs for samples graphitized at 1100 °C. In other words, high performance Co/C (Co_3O_4/C) NPCs for ORR and/or OER or *vice versa* can be realized by simply switching of the graphitization conditions. This is the first time that such an effective approach has been developed from a single source MOF or ZIF structure; typically additional factors such as extra functional precursor or carbon support or post-synthesis treatment are required. Our synthesis method only involves direct graphitization without the addition of any other functional precursors or extensive chemical treatment. Simple control over graphitization and cobalt-concentration produce balanced graphitic, nitrogen doped and cobalt embedded NPCs. These show highly effective catalytic performance for ORR and OER, equivalent to or better than benchmark Pt/C and IrO_2/C. From calculations of the energy diagram under an applied voltage V we identify that the ORR reaction is significantly more exothermic for mixed cobalt–nitrogen doped systems than pure graphitic system. The reactivity (and thus efficiency) of the complete electrochemical cycle can be modified by tuning of the nitrogen content. Finally, characterization reveals that for ORR nitrogen doping and cobalt concentration are primarily responsible for yielding notably more positive onset potentials. In contrast, for OER the combined graphitization and fine dispersion of cobalt metal concentration defines the reaction kinetics and the overall performance. Porosity with fine dispersion of active sites is the key in enhancing the overall activity. The results reported here can guide further advancement in targeted synthesis of nanoporous carbon-based high-performance bifunctional catalysts for high capacity metal–air batteries and overall water splitting.

Acknowledgements

References

1   M. M. Thackeray, C. Wolverton and E. D. Isaacs, Electrical energy storage for transportation—approaching the limits of, and going beyond, lithium-ion batteries, *Energy Environ. Sci.*, 2012, **5**, 7854.

2   The International Renewable Energy Agency (IRENA): Smart grids and Renewables – A Guide for Effective Deployment, http://www.irena.org/documentdownloads/publications/smart_grids.pdf.

3   L. Dai, Y. Xue, L. Qu, H.-J. Choi and J.-B. Baek, Metal-free catalysts for oxygen reduction reaction, *Chem. Rev.*, 2015, **115**, 4823.

4   H. Furukawa, K. E. Cordova, M. O'Keeffe and O. M. Yaghi, The chemistry and applications of metal–organic frameworks, *Science*, 2013, **341**, 1230444.

5   G. Férey, Hybrid porous solids: past, present, future, *Chem. Soc. Rev.*, 2008, **37**, 191.

6   S. Gadipelli and Z. X. Guo, Graphene-based materials: synthesis and gas sorption, storage and separation, *Prog. Mater. Sci.*, 2015, **69**, 1.

7   J.-K. Sun and Q. Xu, Functional materials derived from open framework templates/precursors: synthesis and applications, *Energy Environ. Sci.*, 2014, **7**, 2071.

8   C. Zhang, W. Lv, Y. Tao and Q.-H. Yang, Towards superior volumetric performance: design and preparation of novel carbon materials for energy storage, *Energy Environ. Sci.*, 2015, **8**, 1390.

9   J. Zhang, Z. Zhao, Z. Xia and L. Dai, A metal-free bifunctional electrocatalyst for oxygen reduction and oxygen evolution reactions, *Nat. Nanotechnol.*, 2015, **10**, 444.

10 A. M. El-Sawy, I. M. Mosa, D. Su, C. J. Guild, S. Khalid, R. Joesten, J. F. Rusling and S. L. Suib, Controlling the active sites of sulfur-doped carbon nanotube–graphene nanolobes for highly efficient oxygen evolution and reduction catalysis, *Adv. Energy Mater.*, 2015, **6**, 1501966.

11 Q. Li, R. Cao, J. Cho and G. Wu, Nanocarbon electrocatalysts for oxygen reduction in alkaline media for advanced energy conversion and storage, *Adv. Energy Mater.*, 2014, **4**, 1301415.

12 Z. Zhao, M. Li, L. Zhang, L. Dai and Z. Xia, Design principles for heteroatom-doped carbon nanomaterials as highly efficient catalysts for fuel cells and metal–air batteries, *Adv. Mater.*, 2015, **27**, 6834.

13 Y. Li and H. Dai, Recent advances in zinc–air batteries, *Chem. Soc. Rev.*, 2014, **43**, 5257.

14 Y. Liang, Y. Li, H. Wang, J. Zhou, J. Wang, T. Regier and H. Dai, Co_3O_4 nanocrystals on graphene as a synergistic catalyst for oxygen reduction reaction, *Nat. Mater.*, 2011, **10**, 780.

15 X. Liu, W. Liu, M. Ko, M. Park, M. G. Kim, P. Oh, S. Chae, S. Park, A. Casimir, G. Wu and J. Cho, Metal (Ni, Co)-metal oxides/graphene nanocomposites as multifunctional electrocatalysts, *Adv. Funct. Mater.*, 2015, **25**, 5799.

16 J. Wang, K. Li, H. Zhong, D. Xu, Z. Wang, Z. Jiang, Z. Wu and X. Zhang, Synergistic effect between metal–nitrogen–carbon sheets and NiO nanoparticles for enhanced electrochemical water-oxidation performance, *Angew. Chem., Int. Ed.*, 2015, **54**, 10530.

17 J. Masa, W. Xia, M. Muhler and W. Schuhmann, On the role of metals in nitrogen-doped carbon electrocatalysts for oxygen reduction, *Angew. Chem., Int. Ed.*, 2015, **54**, 10102.

18 X. Liu, M. Park, M. G. Kim, S. Gupta, G. Wu and J. Cho, Integrating NiCo alloys with their oxides as efficient bifunctional cathode catalysts for rechargeable zinc–air batteries, *Angew. Chem., Int. Ed.*, 2015, **54**, 9654.

19 J. Xie, X. Yao, Q. Cheng, I. P. Madden, P. Dornath, C.-C. Chang, W. Fan and D. Wang, Three dimensionally ordered mesoporous carbon as a stable, high-performance Li–O_2 battery cathode, *Angew. Chem.*, 2015, **127**, 4373.

20 T. Y. Ma, J. L. Cao, M. Jaroniec and S. Z. Qiao, Interacting carbon nitride and titanium carbide nanosheets for

high-performance oxygen evolution, *Angew. Chem., Int. Ed.*, 2015, **55**, 1138.

21 M. Ledendecker, G. Clavel, M. Antonietti and M. Shalom, Highly porous materials as tunable electrocatalysts for the hydrogen and oxygen evolution reaction, *Adv. Funct. Mater.*, 2015, **25**, 393.

22 Y.-Z. Chen, C. Wang, Z.-Y. Wu, Y. Xiong, Q. Xu, S.-H. Yu and H.-L. Jiang, From bimetallic metal–organic framework to porous carbon: high surface area and multicomponent active dopants for excellent electrocatalysis, *Adv. Mater.*, 2015, **27**, 5010.

23 W. Xia, R. Zou, L. An, D. Xia and S. Guo, A metal–organic framework route to in situ encapsulation of Co@Co$_3$O$_4$@C core@bishell nanoparticles into a highly ordered porous carbon matrix for oxygen reduction, *Energy Environ. Sci.*, 2015, **8**, 568.

24 B. Y. Xia, Y. Yan, N. Li, H. B. Wu, X. W. Lou and X. Wang, A metal–organic framework-derived bifunctional oxygen electrocatalyst, *Nat. Energy*, 2016, **1**, 15006.

25 K. Strickland, E. Miner, Q. Jia, U. Tylus, N. Ramaswamy, W. Liang, M.-T. Sougrati, F. Jaouen and S. Mukerjee, Highly active oxygen reduction non-platinum group metal electrocatalyst without direct metal–nitrogen coordination, *Nat. Commun.*, 2015, **6**, 7343.

26 S. You, X. Gong, W. Wang, D. Qi, X. Wang, X. Chen and N. Ren, Enhanced cathodic oxygen reduction and power production of microbial fuel cell based on noble-metal-free electrocatalyst derived from metal–organic frameworks, *Adv. Energy Mater.*, 2015, **6**, 1501497.

27 B. You, N. Jiang, M. Sheng, W. S. Drisdell, J. Yano and Y. Sun, Bimetal–organic framework self-adjusted synthesis of support-free nonprecious electrocatalysts for efficient oxygen reduction, *ACS Catal.*, 2015, **5**, 7068.

28 S. Gadipelli and Z. X. Guo, Tuning of MOF-derived carbon with high activity, nitrogen functionality and yield – a case for superior CO$_2$ capture, *ChemSusChem*, 2015, **8**, 2123.

29 G. Srinivas, V. Krungleviciute, Z.-X. Guo and T. Yildirim, Exceptional CO$_2$ capture in a hierarchically porous carbon with simultaneous high surface area and pore volume, *Energy Environ. Sci.*, 2014, **7**, 335.

30 K. S. Park, Z. Ni, A. P. Cote, J. Y. Choi, R. Huang, F. J. Uribe-Romo, H. K. Chae, M. O'Keeffe and O. M. Yaghi, Exceptional chemical and thermal stability of zeolitic imidazolate frameworks, *Proc. Natl. Acad. Sci. U. S. A.*, 2006, **103**, 10186.

31 H. Li, M. Eddaoudi, M. O'Keeffe and O. M. Yaghi, Design and synthesis of an exceptionally stable and highly porous metal–organic framework, *Nature*, 1999, **402**, 276.

32 G. Srinivas, C. A. Howard, S. M. Bennington, N. T. Skipper and M. Ellerby, Effect of hydrogenation on structure and superconducting properties of CaC$_6$, *J. Mater. Chem.*, 2009, **19**, 5239.

33 G. Srinivas, A. Lovell, N. T. Skipper, S. M. Bennington, K. Zynep and R. I. Smith, Ammonia absorption in calcium graphite intercalation compounds: in situ neutron diffraction, Raman spectroscopy and magnetization, *Phys. Chem. Chem. Phys.*, 2010, **12**, 6253.

34 S. Gadipelli, H. A. Patel and Z. X. Guo, An ultrahigh pore volume drives up amine stability and cyclic CO$_2$ capacity of a solid-amine@carbon sorbent, *Adv. Mater.*, 2015, **27**, 4903.

35 S. Gadipelli, W. Travis, W. Zhou and Z. Guo, A thermally derived and optimized structure of ZIF-8 with giant enhancement in CO$_2$ uptake, *Energy Environ. Sci.*, 2014, **7**, 2232.

36 G. Srinivas, J. Burres and T. Yildirim, Graphene oxide derived carbons (GODCs): synthesis and gas adsorption properties, *Energy Environ. Sci.*, 2012, **5**, 6453.

37 G. Srinivas, Y. Zhu, R. Piner, N. Skipper, M. Ellerby and R. Ruoff, Synthesis of graphene-like nanosheets and their hydrogen adsorption capacity, *Carbon*, 2010, **48**, 630.

38 S. Guo, S. Zhang, L. Wu and S. Sun, Co/CoO nanoparticles assembled on graphene for electrochemical reduction of oxygen, *Angew. Chem., Int. Ed.*, 2012, **51**, 11770.

39 K. Xie, J. Masa, E. Madej, F. i. Yang, P. Weide, W. Dong, M. Muhler, W. Schuhmann and W. Xia, Co$_3$O$_4$–MnO$_2$–CNT hybrids synthesized by HNO$_3$ vapor oxidation of catalytically grown CNTs as OER electrocatalysts, *ChemCatChem*, 2015, **7**, 3027.

40 P. Chen, K. Xu, Z. Fang, Y. Tong, J. Wu, X. Lu, X. Peng, H. Ding, C. Wu and Y. Xie, Metallic Co$_4$N porous nanowire arrays activated by surface oxidation as electrocatalysts for the oxygen evolution reaction, *Angew. Chem., Int. Ed.*, 2015, **54**, 14710.

41 W. Chaikittisilp, N. L. Torad, C. Li, M. Imura, N. Suzuki, S. Ishihara, K. Ariga and Y. Yamauchi, Synthesis of nanoporous carbon–cobalt-oxide hybrid electrocatalysts by thermal conversion of metal–organic frameworks, *Chem. – Eur. J.*, 2014, **20**, 4217.

42 J.-S. Li, S.-L. Li, Y.-J. Tang, M. Han, Z.-H. Dai, J.-C. Bao and Y.-Q. Lan, Nitrogen-doped Fe/Fe$_3$C@graphitic layer/carbon nanotube hybrids derived from MOFs: efficient bifunctional electrocatalysts for ORR and OER, *Chem. Commun.*, 2015, **51**, 2710.

43 B. Chen, R. Li, G. Ma, X. Gou, Y. Zhu and Y. Xia, Cobalt sulfide/N,S codoped porous carbon core–shell nanocomposites as superior bifunctional electrocatalysts for oxygen reduction and evolution reactions, *Nanoscale*, 2015, **7**, 20674.

44 X. Li, Y. Fang, X. Lin, M. Tian, X. An, Y. Fu, R. Li, J. Jin and J. Ma, MOF derived Co$_3$O$_4$ nanoparticles embedded in N-doped mesoporous carbon layer/MWCNT hybrids: extraordinary bi-functional electrocatalysts for OER and ORR, *J. Mater. Chem. A*, 2015, **3**, 17392.

45 Y. Zhao, R. Nakamura, K. Kamiya, S. Nakanishi and K. Hashimoto, Nitrogen-doped carbon nanomaterials as non-metal electrocatalysts for water oxidation, *Nat. Commun.*, 2013, **4**, 2390.

46 X. Yu, M. Zhang, J. Chen, Y. Li and G. Shi, Nitrogen and sulfur codoped graphite foam as a self-supported metal-free electrocatalytic electrode for water oxidation, *Adv. Energy Mater.*, 2015, **6**, 1501492.

47 S. Cobo, J. Heidkamp, P.-A. Jacques, J. Fize, V. Fourmond, L. Guetaz, B. Jousselme, V. Ivanova, H. Dau, S. Palacin, M. Fontecave and V. Artero, A Janus cobalt-based catalytic material for electro-splitting of water, *Nat. Mater.*, 2012, **11**, 802.

This journal is © The Royal Society of Chemistry 2016

Energy Environ. Sci., 2016, **9**, 1661–1667 | **1667**